

# Hydrogen-Bonded Homoleptic Fluoride–Diarylurea Complexes: Structure, Reactivity, and Coordinating Power

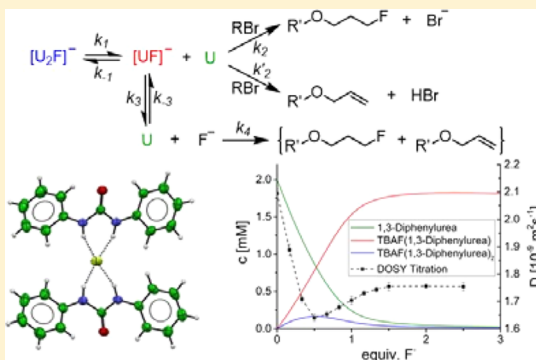
Lukas Pfeifer,<sup>†</sup> Keary M. Engle,<sup>†,§</sup> George W. Pidgeon,<sup>†</sup> Hazel A. Sparkes,<sup>‡,||</sup> Amber L. Thompson,<sup>†</sup> John M. Brown,<sup>†</sup> and Véronique Gouverneur<sup>\*,†</sup>

<sup>†</sup>Chemistry Research Laboratory, University of Oxford, 12 Mansfield Road, OX1 3TA Oxford, United Kingdom

<sup>‡</sup>ISIS Facility, STFC-Rutherford Appleton Laboratory, OX11 0QX Didcot, United Kingdom

## Supporting Information

**ABSTRACT:** Hydrogen bonding with fluoride is a key interaction encountered when analyzing the mode of action of 5'-fluoro-5'-deoxyadenosine synthase, the only known enzyme capable of catalyzing the formation of a C–F bond from F<sup>−</sup>. Further understanding of the effect of hydrogen bonding on the structure and reactivity of complexed fluoride is therefore important for catalysis and numerous other applications, such as anion supramolecular chemistry. Herein we disclose a detailed study examining the structure of 18 novel urea–fluoride complexes in the solid state, by X-ray and neutron diffraction, and in solution phase and explore the reactivity of these complexes as a fluoride source in S<sub>N</sub>2 chemistry. Experimental data show that the structure, coordination strength, and reactivity of the urea–fluoride complexes are tunable by modifying substituents on the urea receptor. Hammett analysis of aryl groups on the urea indicates that fluoride binding is dependent on  $\sigma_p$  and  $\sigma_m$  parameters with stronger binding being observed for electron-deficient urea ligands. For the first time, defined urea–fluoride complexes are used as fluoride-binding reagents for the nucleophilic substitution of a model alkyl bromide. The reaction is slower in comparison with known alcohol–fluoride complexes, but S<sub>N</sub>2 is largely favored over E2, at a ratio surpassing all hydrogen-bonded complexes documented in the literature for the model alkyl bromide employed. Increased second-order rate constants at higher dilution support the hypothesis that the reactive species is a 1:1 urea–fluoride complex of type [UF]<sup>−</sup> (U = urea) resulting from partial dissociation of the parent compound [U<sub>2</sub>F]<sup>−</sup>. The dissociation processes can be quantified through a combination of UV and NMR assays, including DOSY and HOESY analyses that illuminate the complexation state and H-bonding in solution.



## INTRODUCTION

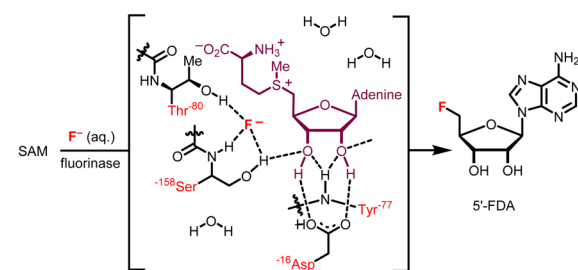
During the past 10 years, chemists have developed new methods to incorporate fluorine into organic molecules by appending carbon–fluorine (C–F) bonds onto aromatic and aliphatic chains.<sup>1</sup> Reactions employing a fluoride source are attractive because fluoride is the most abundant form of the element on earth.<sup>2</sup> In nucleophilic substitution, the difficulties associated with fluoride chemistry are usually related to the poor solubility of common fluoride salts in organic solvents and the ability of fluoride to form strong hydrogen bonds with functional groups commonly found on organic substrates, for example alcohols, amines, or amides. These interactions can attenuate fluoride nucleophilicity,<sup>3</sup> thereby limiting access to C–F bond formation via nucleophilic substitution reactions. In the absence of hydrogen-bond donors, fluoride basicity can override its nucleophilicity, leading to unwanted side reactions. In this context, the ultimate challenge in terms of fluoride reactivity is to form a C–F bond from fluoride in an aqueous medium. Nature has evolved a fluorinase enzyme, 5'-fluoro-5'-deoxyadenosine synthase, capable of catalyzing the reaction of S-adenosyl-L-methionine (SAM) and a fluoride ion to generate 5'-fluorodeoxyadenosine (5'-FDA) and L-methionine.<sup>4</sup> Inspec-

tion of the active site of this enzyme and detailed studies of its mode of action indicate that in the first instance fluoride ( $K_M \approx 10$  mM) exchanges four hydrogen-bonded water molecules for hydrogen-bonding contacts to Ser-158; subsequent binding of SAM ( $K_M \approx 10$   $\mu$ M) induces complete fluoride desolvation along with concomitant formation of an additional hydrogen-bonding contact with Thr-80 and exposure of the fourth coordination site of fluoride to the electropositive sulfonium leaving group positioned at the 5'C-carbon of SAM.<sup>5</sup> This tricoordinated fluoride remains a good nucleophile (Figure 1A).<sup>6</sup> The paucity of information regarding the relationship between hydrogen bonding (i.e., the nature of the hydrogen-bond donor and the coordination number) and fluoride reactivity has prompted us to undertake a systematic study, in which we have examined the binding of H-bond donors to the fluoride ion to control its nucleophilicity (Figure 1B).<sup>3,7,8</sup> Our long-term objective is to organize the coordination environment around the fluoride ion so as to enable its nucleophilic chemistry to occur in an asymmetric environment and thus

Received: July 27, 2016

Published: September 8, 2016

A. Fluorinase enzyme showing tricoordinated fluoride ion within the active site



B. Coordination diversity and reactivity of homoleptic alcohol–fluoride complexes

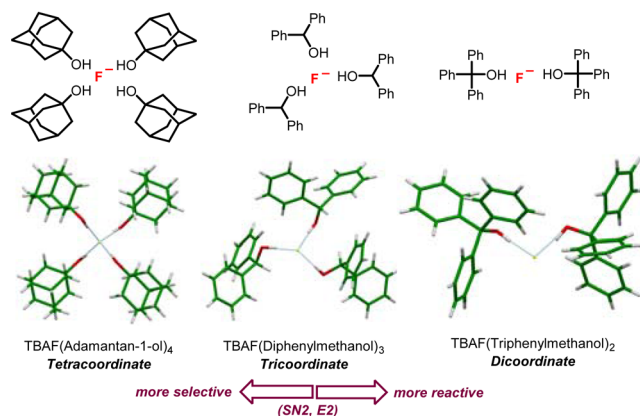


**Figure 1.** Coordination diversity in hydrogen-bonded fluoride complexes. (A) 5'-Fluoro-5'-deoxyadenosine synthase. (B) Structure and reactivity of alcohol–fluoride complexes.

function as a viable model for the enzyme fluorinase. Our first paper showed the variety of ways in which alcohols coordinate to fluoride and the consequences of the coordination mode on  $S_N2$  reactivity.<sup>9</sup> This study was largely based on a broad-ranging set of crystal structures that revealed varying coordination numbers for the alcohol ligand and fluctuations in the geometry of the coordination sphere. The present investigation likewise examines the structure and reactivity of hydrogen-bonded homoleptic fluoride–urea complexes.

1,3-Diarylureas have found widespread use in diverse areas of chemistry as anion receptors,<sup>10</sup> sensors,<sup>11</sup> and gelating agents,<sup>12</sup> as well as in the fields of molecular recognition<sup>13</sup> and organocatalysis.<sup>14</sup> These studies have involved a full range of spectroscopic tools, with structural characterization of key hydrogen-bonding interactions by single-crystal X-ray diffraction. These insights have led to the successful design of reagents for specific binding of simple inorganic ions that are medically important, including chloride and nitrate. The strong H-bonding ability of the urea group has also been explored to control the configuration of foldamers and to induce and control helicity in polymers.<sup>15</sup> There are some examples of characterized urea–fluoride complexes in the literature, where interest has largely centered on bi- and tripodal ligands that enforce specific coordination geometries.<sup>16</sup> The species involved are of interest as colorimetric sensors. Herein, we report the synthesis of a defined set of novel 1,3-diarylurea–fluoride complexes and their characterization by single-crystal X-ray and neutron diffraction as well as in solution, and we demonstrate that these complexes are suitable reagents for C–F bond formation on aliphatic chains by nucleophilic substitution. Structure, reactivity, and product

selectivity can be fine-tuned through structural variation of the urea ligand.

## RESULTS AND DISCUSSION

**I. Synthesis and Characterization of Hydrogen-Bonded Fluoride–Urea Complexes.** At the commencement of this study, only one crystal structure of a simple 1,3-diarylurea–fluoride complex had been reported,<sup>17</sup> along with others that employ this motif within a chelating template. The previously reported structure was derived from a reaction of 1,3-bis(4-nitrophenyl)urea with TMAF affording a 2:1 urea/fluoride complex  $[U_2F]^-$  (U = urea), a stoichiometry that differs from complexes derived from chloride or acetate.

The ureas selected in the present study were chosen on the basis of varied aryl substituents to examine any influence of steric and electronic effects on coordination geometries in the solid state. The complexes were prepared in good yields by adapting an established synthetic protocol (Table 1);

**Table 1.** 1,3-Diarylurea–Fluoride Complexes 2a–r As Characterized Using Single-Crystal X-ray Diffraction

$$\text{TBAF}(\text{H}_2\text{O})_3 \xrightarrow[\text{hexane, 85 } ^\circ\text{C, 2 h}]{\text{urea (2.0 equiv.)}} \text{TBAF}(\text{urea})_n$$

entry	urea	yield	complex	type	C.N. <sup>a</sup>
1	1a, R = 3-CH <sub>3</sub>	87%	2a	A <sub>1</sub>	2
2	1b, R = 4-CF <sub>3</sub>	96%	2b	A <sub>1</sub>	2
3	1c, R = 4-NO <sub>2</sub>	96%	2c	A <sub>1</sub>	2
4	1d, R = 4- <i>n</i> -Pr	97%	2d <sup>b</sup>	A <sub>1</sub>	2
5	1e, R = 4-H	90%	2e	A <sub>2</sub>	2
6	1f, R = 4-CH <sub>3</sub>	97%	2f	A <sub>2</sub>	2
7	1g, R = 4-OCH <sub>3</sub>	91%	2g	A <sub>2</sub>	2
8	1h, R = 4-Cl	99%	2h <sup>b</sup>	A <sub>2</sub>	2
9	1i, R = 4- <i>n</i> -Bu	77%	2i	A <sub>2</sub>	2
10	1j, R = 4-F	94%	2j <sup>b</sup>	B	2
11	1k, R = 4- <i>i</i> -Pr	94%	2k	B	2
12	1l, R = 4-I	91%	2l	C	1 <sup>c</sup>
13	1m, R = 4-Br	97%	2m	C	1 <sup>c</sup>
14	1n, R = 4-Et	95%	2n	C	1 <sup>c</sup>
15	1k, R = 4- <i>i</i> -Pr	94%	2o	C	1 <sup>c</sup>
16	1m, R = 4-Br	97%	2p <sup>d</sup>	C	1 <sup>c</sup>
17	1e, R = 4-H (NMe <sub>4</sub> <sup>+</sup> )	99%	2q	D	3
18	1e, R = 4-H (NEt <sub>4</sub> <sup>+</sup> )	98%	2r	D	3

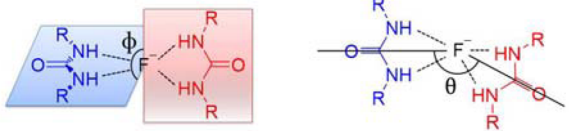
<sup>a</sup>Coordination number  $n$  for  $(\text{urea})_n\text{F}^-$ . <sup>b</sup>Neutron diffraction structure also obtained. <sup>c</sup> $[\text{urea}/\text{H}_2\text{O}/\text{F}^-] = 1:1:1$ . <sup>d</sup>CH<sub>2</sub>Cl<sub>2</sub> solvate. TBAF = tetrabutylammonium fluoride.

TBAF·3H<sub>2</sub>O was combined with the urea (2 equiv) in vigorously refluxing hexane for 2 h.<sup>9</sup> The ensuing crude solid materials were characterized by <sup>1</sup>H and <sup>13</sup>C NMR as well as IR spectroscopy, and recrystallized as appropriate to obtain single-crystals suitable for X-ray diffraction studies. In addition to TBAF·3H<sub>2</sub>O, TMAF·4H<sub>2</sub>O and TEAF·2H<sub>2</sub>O were also employed for the preparation of complexes from 1,3-diphenylurea 1e. Complete synthetic procedures can be found in the Supporting Information (SI).

In the 2:1 urea–fluoride complexes, the fluoride adopts a position approximately equidistant between two urea molecules, acting as a doubly bifurcated hydrogen-bond acceptor. This  $[U_2F]^-$  motif can be characterized by the urea–urea interplanar angle ( $\phi$ ) and the O···F···O angle ( $\theta$ ), whereby

changes to these angles lead to differences in the fluoride coordination geometry. Due to steric restrictions this can range from square planar ( $\phi = 0^\circ$ ,  $\theta = 180^\circ$ ), to tetrahedral ( $\phi = 90^\circ$ ,  $\theta = 180^\circ$ ) and tetragonal pyramidal with a vacant apical site ( $\phi = <90^\circ$ ,  $\theta = <180^\circ$ ) (Table 2).

**Table 2. Summary of Urea–Urea Interplanar Angles ( $\phi$ ) Described by the NNCO Motif, and  $O\cdots F\cdots O$  Angles ( $\theta$ ) for Complexes of Types A and C**



entry	complex	$\phi$ [deg]	$\theta$ [deg]	$S_p/T_d/T_p^a$
1	2a	59.66(9)	131.88(4)	$T_p$
2	2b	56.3(4)	137.55(12)	$T_p$
3	2c	4.26(15)	172.60(5)	$S_p$
4	2d	15.52(9)	163.11(4)	$S_p-T_p$
5	2e	43.15(9)	169.87(4)	$S_p-T_d$
		64.13(7)	173.54(3)	$S_p-T_d$
6	2f	43.12(12)	174.12(5)	$S_p-T_d$
		77.58(10)	171.69(5)	$T_d$
7	2g	80.9(2)	174.71(9)	$T_d$
		maj.: 43.5(4)	maj.: 177.10(15)	$S_p-T_d$
		min.: 38.8(7)	min.: 172.49(17)	
8	2h	76.27(7)	172.23(3)	$T_d$
		40.59(9)	172.71(4)	$S_p-T_d$
9	2i	27.41(15)	155.00(5)	$T_p$
		16.52(17)	168.58(7)	$T_p$
10 <sup>b</sup>	2l	60.99(18)	144.51(6) <sup>c</sup>	–
11 <sup>b</sup>	2m	68.5(2)	138.72(7) <sup>c</sup>	–
12 <sup>b</sup>	2n	0 <sup>d</sup>	180 <sup>c,d</sup>	–
13 <sup>b</sup>	2o	6.60(15)	175.55(4) <sup>c</sup>	–
14 <sup>b</sup>	2p	0 <sup>d</sup>	180 <sup>c,d</sup>	–

<sup>a</sup> $S_p$  = square planar,  $T_d$  = tetrahedral,  $T_p$  = tetragonal pyramidal with vacant apical site. <sup>b</sup>Two ureas binding to one  $(F^- \cdot H_2O)_2$  dianion used. <sup>c</sup>Centroid between the two fluorides of the  $(F^- \cdot H_2O)_2$  dianion used as hinge point. <sup>d</sup>Ureas related by inversion.

For a relatively restricted set of substrates, a surprisingly rich and variable set of crystal structures were obtained, revealing several distinct modes of coordination. Many of the structures adopt the known  $[U_2F]^-$  motif described above (A), but significant structural variations were unveiled within this series prompting us to further subdivide this category to distinguish between types  $A_1$  and  $A_2$ . Three additional modes of complexation were identified, consisting of  $[U_4F_2]^{2-}$  complexes of type B,  $[U_2(H_2O)_2F_2]^{2-}$  complexes of type C, and  $[U_3F]^-$  complexes of type D (Figure 2).

This diversity of structural arrangements encountered in the solid state is unprecedented for ureas and deserves detailed commentary.

**Type  $A_1$  2:1 Structures.** Structures of type  $A_1$  (2a–d) have a single ion-pair structure within the unit cell, forming the previously described  $[U_2F]^-$  motif. The simplest type of structure observed involves a single 2:1 fluoride anion urea complex with defined geometry and four  $NH\cdots F^-$  hydrogen bonds. The interurea interplanar angle varies widely, though this is probably largely directed by crystal packing forces.<sup>18</sup> For 3-Me and 4- $CF_3$  substituted complexes (2a and 2b), the  $O\cdots$

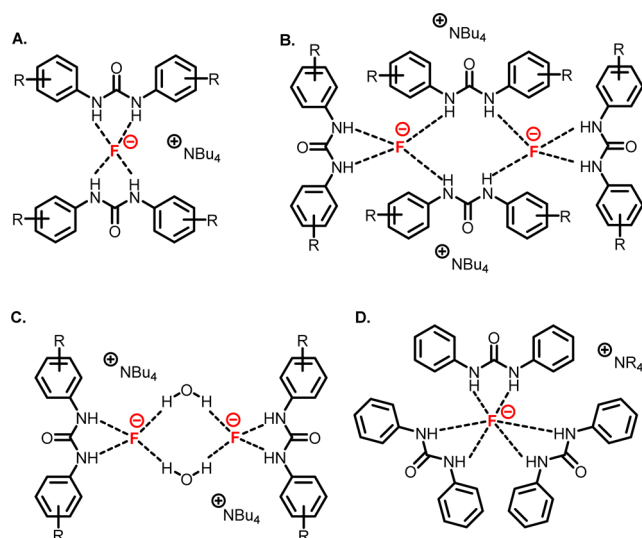


**Figure 2. Coordination diversity of urea–fluoride complexes. (A) Type A complexes,  $[U_2F]^-$ . (B) Type B complexes,  $[U_4F_2]^{2-}$ . (C) Type C complexes,  $[U_2(H_2O)_2F_2]^{2-}$ . (D) Type D complexes,  $[U_3F]^-$ .**

$F^- \cdots O$  angle deviates significantly from linearity such that all four N–H hydrogen-bond donors lie within the same hemisphere forming a tetragonal pyramid (Table 2, entries 1 and 2), where the vacant site is occupied by weak, long-range C–H donors. This had been observed previously for the 2:1 pinacol–fluoride ion complex.<sup>9</sup> Complexes 2c (4- $NO_2$ ) and 2d (4- $n$ -Pr) show shallow interplanar angles of  $4.26(15)^\circ$  and  $15.52(9)^\circ$ , respectively, making them more square planar (Table 2, entries 3 and 4).

**Type  $A_2$  2:1 Structures.**  $A_2$ -type structures (2e–i) possess two crystallographically distinct ion pairs with different twist geometries, exemplified by Figure 3. The substitution of Me

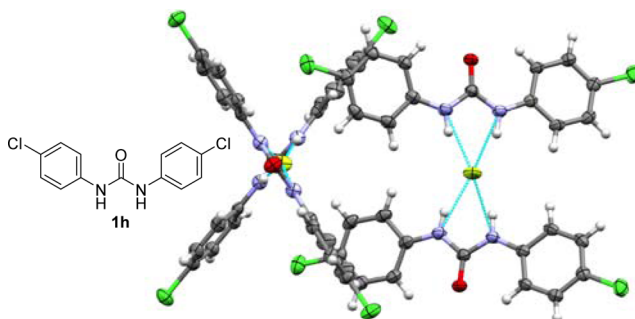


**Figure 3. Solid state structure of the two independent  $[U_2F]^-$  anions in 2h determined using single-crystal X-ray diffraction; urea–urea interplanar angles are  $40.59(9)^\circ$  and  $76.27(7)^\circ$ . Displacement ellipsoid plot drawn at 50% probability; cations are omitted for clarity.**

(2f) with Cl (2h) gives an isomorphous pair of structures, which is consistent with the previously described “chloromethyl exchange rule”.<sup>19</sup> Structures 2e (4-H) and 2g (4-OMe) are very similar and can be said to be isostructural.<sup>20</sup> Individual ion pairs are chiral, possessing  $C_2$  symmetry by virtue of their twist about the  $O=C\cdots F^- \cdots C=O$  axis; the two closest ion pairs in each structure have different twist angles about this axis but in the same sense. This assembly together with its enantiomer makes up a half unit cell. Their  $O\cdots F^- \cdots O$  angles are close to linearity, and with interurea interplanar angles between  $40^\circ$  and  $81^\circ$ , their coordination geometry can be

described either as tetrahedral or as an intermediary state between square planar and tetrahedral (Table 2, entries 5–8). Complex **2i** (4-*n*-Bu) stands out, for two separate complexes are observed where the paired anionic ligands describe a shallow V-shape, forming a tetragonal pyramidal coordination sphere with interplanar urea angles of 16.52(17)° and 27.41(15)°, respectively (Table 2, entry 9). This is also characterized by the O···F<sup>-</sup>···O angles' distinct deviation from linearity.

**Type B 4:2 Structures.** These involve a supramolecular 4:2 structure (Figure 4). Each of the two fluoride ions has a total of

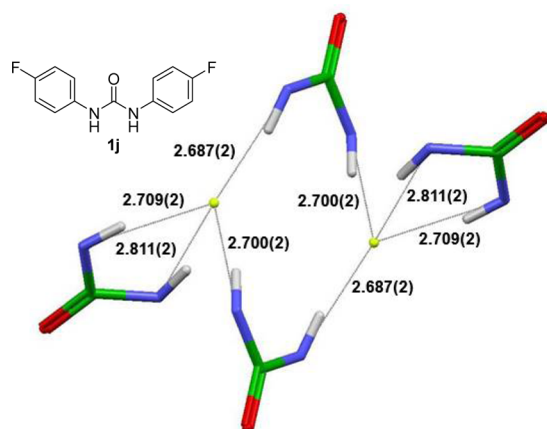


**Figure 4.** Bridging and terminal urea bonding in the 4:2 supramolecular fluoride complex **2j** from 1,3-bis(4-fluorophenyl)urea **1j**. N(H)···F<sup>-</sup> distances are shown. Aryl groups and cations are omitted for clarity.

four H-bonds arising from interactions with three urea molecules. One terminal urea provides two H-bond contacts, while the other two ureas bridge the two fluorides, providing one H-bond contact each. All the H-bonds are short, with N(H)···F<sup>-</sup> distances ≤2.82 Å. Structure **2j** (4-F) in Figure 4 has a F<sup>-</sup>···F<sup>-</sup> distance of 3.2632(16) Å, and **2k** (4-*i*-Pr) likewise 3.045(3) Å. This type of [U<sub>4</sub>F<sub>2</sub>]<sup>2-</sup> structure, with a bridging bifunctional H-bonding ligand, is without precedent in the Cambridge Structural Database.<sup>21</sup>

For **2j**, it was possible to grow a crystal suitable for single-crystal neutron diffraction, which allowed the accurate determination and comparison of the four NH···F<sup>-</sup> H-bond lengths and angles. It was also possible to grow similarly large crystals of the 4-*n*-Pr (**2d**, A<sub>1</sub>) and 4-Cl (**2h**, A<sub>2</sub>) substituted

urea complexes, so the parameters of three structures could be compared with those obtained from the X-ray data (Table 3). Hydrogen-bond angles are thereby determined to be in the range 152°–166°, displaying a clear deviation from ideal linearity due to the bite angle of the urea motif.

**Type C 2:2 Dihydrate Structures.** For the urea complexes above, variations in the aryl side chain led only to products with 2:1 urea/fluoride stoichiometry. Synthesis involving *p*-iodinated ligand **1l** as before, however, gave **2l**, which included water of crystallization (Figure 5). This presumably originated from TBAF·3H<sub>2</sub>O, despite the fact that the reaction was conducted with azeotropic water removal.

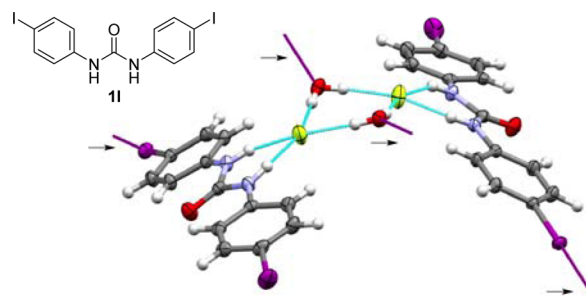


**Figure 5.** Anionic component of structure **2l**; → shows the vectors of I···O halogen bonding. Displacement ellipsoid plot drawn at 50% probability; cations are omitted for clarity.

A similar product **2m** is formed from the corresponding bromide **1m**. There are single I···O and Br···O halogen-bonding interactions between neighboring urea ligands and both water molecules in **2l** and **2m**.<sup>22</sup> For **2l**, the I···O distance is 3.037(2) Å, and in **2m**, the Br···O distance is 3.090(3) Å. The C–Hal···O angles are 174.37(10)° and 170.84(15)°, respectively. The approximately linear geometries are indicative of an interaction between the positively polarized covalently bonded terminal halogen substituent and negatively polarized oxygen along the direction of the R–Hal bond. Side-chain bulk is also an important factor, since a closely related complex **2o** is formed from the *p*-*i*-Pr-substituted urea **1k**. The fourth member of this subgroup, **2p**, is an alternative structure derived from bromide **1m** that includes CH<sub>2</sub>Cl<sub>2</sub> of crystallization and does not display the aforementioned halogen-bonding interactions found in **2m**. Complex **2n** bearing *p*-Et substituents on the phenyl groups of the urea stood out, as the crystal was found to be aperiodic.<sup>23</sup> Across these structures, the average F<sup>-</sup>···F<sup>-</sup> distance is 4.17 ± 0.031 Å, and the central water–fluoride unit

**Table 3.** Hydrogen-Bonding Distances and Angles for **2d**, **2h**, and **2j** from Single-Crystal X-ray and Neutron Diffraction Data

complex	D–H [Å]	H···A [Å]	D···A [Å]	∠DHA [deg]
<b>2d</b> , R = 4- <i>n</i> -Pr, X-ray/neutron	0.863/1.049(9)	1.893(2)/1.696(9)	2.7004(15)/2.697(6)	155/158.0(8)
	0.867/1.007(11)	1.880(2)/1.750(11)	2.6994(16)/2.704(6)	157/156.6(8)
	0.856/1.043(10)	1.915(2)/1.731(10)	2.7261(17)/2.716(6)	158/155.7(9)
	0.838/1.013(11)	1.978(2)/1.796(10)	2.7631(17)/2.747(6)	156/154.8(8)
<b>2h</b> , R = 4-Cl, X-ray/neutron	0.850/1.046(9)	1.834(1)/1.634(9)	2.6538(11)/2.648(4)	162/161.8(9)
	0.852/1.042(10)	2.011(1)/1.825(10)	2.7945(10)/2.788(4)	153/152.0(8)
	0.848/1.013(15)	1.879(1)/1.719(13)	2.6821(11)/2.672(6)	157/155.2(9)
	0.878/1.012(14)	1.872(1)/1.748(14)	2.6989(11)/2.697(5)	156/154.6(9)
<b>2j</b> , R = 4-F, X-ray/neutron	0.856/1.030(10)	1.853(2)/1.674(10)	2.6866(19)/2.676(6)	164/162.8(9)
	0.861/1.062(8)	1.858(2)/1.659(9)	2.700(2)/2.700(6)	165/165.7(10)
	0.856/1.031(15)	1.881(2)/1.703(14)	2.7086(19)/2.698(8)	162/160.8(9)
	0.862/1.062(13)	2.002(2)/1.820(13)	2.811(2)/2.807(8)	156/153.0(9)

is approximately planar. The dihedral angles between urea planes in **2l** and **2m** are  $60.99(18)^\circ$  and  $68.5(2)^\circ$ , and together with  $\theta$  values of  $144.51(6)^\circ$  and  $138.72(7)^\circ$ , they describe the shallow U-shape that is formed by the hydrogen-bonded assembly (Table 2, entries 10 and 11). In contrast, the urea planes in structures **2n–p** are parallel or almost parallel, and  $\theta$  shows a perfectly or almost linear relationship between the two carbonyl oxygens and the centroid between the two fluoride anions (Table 2, entries 12–14). The Cambridge Structural Database (CSD)<sup>21</sup> reveals several examples of  $(F^- \cdot H_2O)_2$  dication clusters, although their generality has not been well recognized, despite Emsley's early discussion.<sup>24,25</sup> Here, their formation in an isolated unit is encouraged in part by the combination of a bulky *p*-substituent in the 1,3-diaryurea and a space-demanding countercation, with further interactions available by halogen bonding to the bridging water.

**Type D 3:1 Structures.** The examples discussed above all have  $n\text{-Bu}_4\text{N}^+$  as the countercation, which is itself quite spatially demanding. This posed a question: how does the countercation influence the overall pattern of urea–fluoride bonding? This led to analysis of the structures of the  $\text{Et}_4\text{N}^+$  and  $\text{Me}_4\text{N}^+$  analogues of the parent urea **1e**. The resulting ion pairs, **2q** and **2r**, are similar but distinct from the 2:1  $n\text{-Bu}_4\text{N}^+$ -derived complex **2e**, in that they possess a third coordinated urea ligand. The structures are unsymmetrical, with six different H-bond lengths, two of which are considerably longer than the norm. Overall, the three pairs of donor atoms arrange to form a distorted paddle-wheel motif (Figure 6).

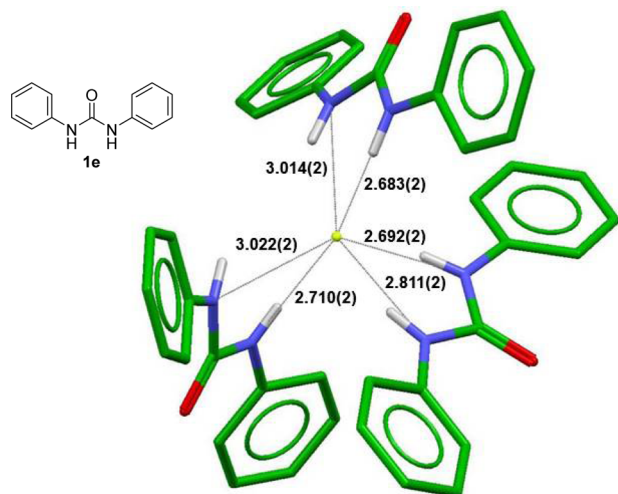


**Figure 6.** H-bonding core for the anionic component of complex **2q** featuring a  $\text{NMe}_4^+$  countercation.  $\text{N(H)} \cdots \text{F}^-$  distances are shown. Aromatic protons and cation are omitted for clarity.

**Other Ligated Fluoride Complexes.** Given the range of structures that are accessible within a rather narrow family of urea-derived complexes, the question of whether the urea unit may be replaced by another H-bonding entity arose. These queries encouraged the synthesis and characterization of four additional fluoride complexes (Table 4).

Fluoride ion complex **4** derived from amide **3** was prepared and crystallized. The X-ray structure demonstrates involvement of the acidic  $\text{C}(\text{sp}^3)\text{-H}$  in H-bonding to fluoride.<sup>26</sup> The most interesting feature of the resulting 2:1 structure is the near colinearity of the  $\text{NH} \cdots \text{F}^-$  H-bonds that are reinforced by two weak  $\text{CH} \cdots \text{F}^-$  bonds, one from the benzhydryl unit and the

**Table 4.** Amide (**4**) and Squaramide (**6a–c**) Complexes Characterized by Single-Crystal X-ray Diffraction

entry	amide	yield	complex	type <sup>a</sup>	C.N. <sup>b</sup>
1	<b>3</b>	93%	<b>4</b>	$\text{A}_1^c$	2
2	<b>5a</b>	98%	<b>6a<sup>d</sup></b>	$\text{A}_1$	2
3	<b>5b</b>	95%	<b>6b</b>	$\text{A}_1$	2
4	<b>5c</b>	96%	<b>6c</b>	$e$	1

<sup>a</sup>See Table 1. <sup>b</sup>Coordination number *n* for  $(\text{amide})_n\text{F}^-$ . <sup>c</sup>With one C–H replacing an N–H. <sup>d</sup>THF solvate. <sup>e</sup>1:1:2 fluoride/squaramide/ $\text{H}_2\text{O}$ .

other less significant one from the proximal *o*-C–H of the arylamide (Figure 7). The amido  $\text{N(H)} \cdots \text{F}^-$  distances at 2.5475(11) and 2.6060(11) Å are shorter than normal values for urea complexes, and all six hydrogen bonds lie in approximately the same plane.

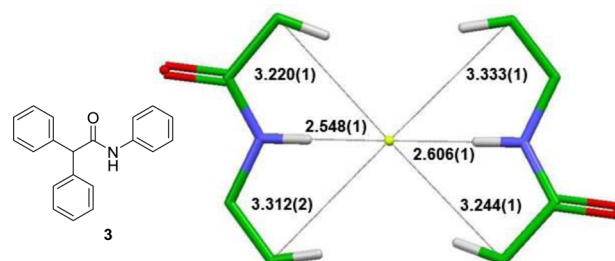


**Figure 7.** Core geometry of the anion of the fluoride ion complex derived from amide **3**, showing  $\text{N(H)} \cdots \text{F}^-$  and  $\text{C(H)} \cdots \text{F}^-$  distances. Aryl groups and cation are omitted for clarity.

Squaramides based on the homologous diamide 1,2-diaminocyclobuten-3,4-dione have been widely utilized in molecular recognition and catalysis.<sup>27</sup> The success of squaramide H-bond donors in these different applications encouraged comparison of the X-ray structures of three prototypical examples with those of related ureas. There are no examples of squaramide–fluoride anion complexes solid state structures in the literature, although several 1:1 chloride anion complexes and one 1:1 bromide anion complex are known.<sup>27b,28</sup> In a direct comparison, transmembrane transport is more efficient for chloride or bicarbonate anions with squaramides than with either analogous ureas or thioureas.<sup>29</sup> The structures of three fluoride ion complexes with squaramides **5a–c** (**6a–c**) were determined by single-crystal X-ray diffraction. Two of these, derived from 4-fluoro and 4-chloro substituted  $N,N'$ -diarylsquaramides **6a** and **6b**, are 2:1 complexes, whereas the parent compound forms a dihydrate (**6c**). For both **6a** and **6b**,  $\text{A}_1$ -type structures are observed (Figure 8). Coplanarity of the two squaramide units is disfavored since the aryl substituents must rotate out of conjugation to avoid a severe steric clash, in contrast to the urea complexes **2a–i**. Consequently they are both twisted out of their common plane with squaramide–squaramide interplanar angles of  $61.48(5)^\circ$  for **6a** and  $78.8(2)^\circ$  for **6b**. Each structure has four distinct short H-bonds, with  $\text{N(H)} \cdots \text{F}^-$  distances in the range 2.637–2.709 Å.

Taken together, this collection of crystal structures provides an extensive set of comparative data on  $\text{N(H)} \cdots \text{F}^-$  distances for ureas and related analogues. The distribution of H-bond

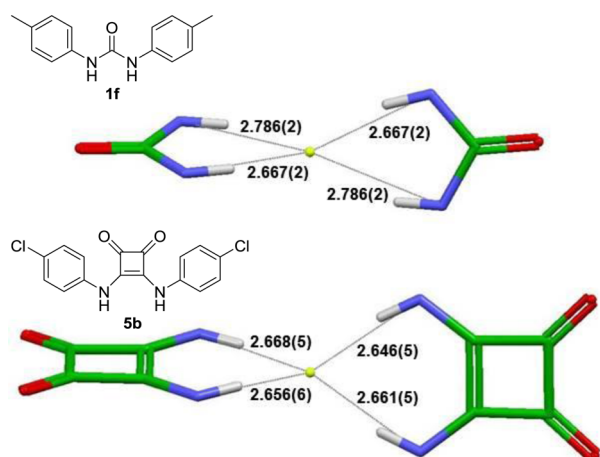


**Figure 8.** Comparative coordination geometries of a typical 2:1 urea (2f) and squaramide (6b) complex. N(H)⋯F<sup>−</sup> distances are shown. Aryl groups and cations are omitted for clarity.

lengths is relatively narrow, and for 2:1 and 4:2 urea–fluoride complexes (A, B; RMS = 2.711 ± 0.062 Å), there is no significant difference in H-bond lengths between electron-rich and electron-poor ureas. Similarly, there is no difference in H-bond lengths between these complexes and 1:1 hydrated urea complexes (C). The average H-bond length is longer, however, in the 3:1 urea–fluoride complexes (D) at RMS = 2.830 ± 0.135 Å (2.754 ± 0.049 Å, omitting the three N(H)⋯F<sup>−</sup> >3.0 Å) and significantly shorter (RMS = 2.662 ± 0.024 Å) in the squaramide complexes. The results are summarized in Figure 9 (see SI for details).

**II. Reactivity of [U<sub>2</sub>F]<sup>−</sup> Complexes in S<sub>N</sub>2 Chemistry.** In our previous paper,<sup>9</sup> it was shown that the coordination state of alcohol–fluoride complexes had a strong effect on both the reactivity and partitioning between S<sub>N</sub>2 and E2 products in a model nucleophilic displacement reaction on a primary alkyl bromide. In the most favorable case, the observed selectivity

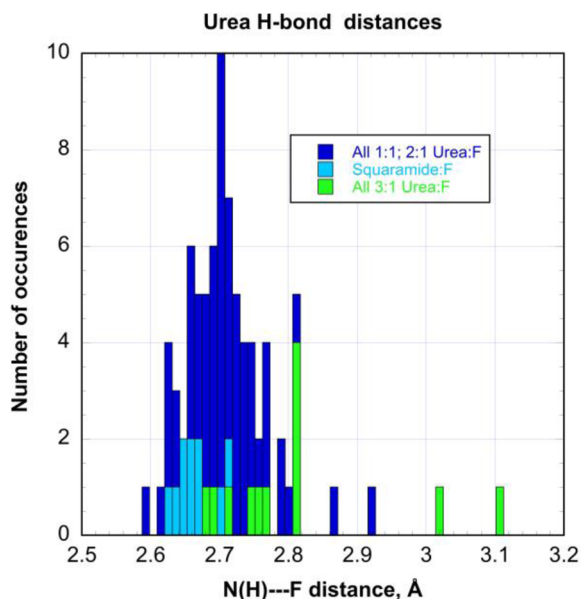
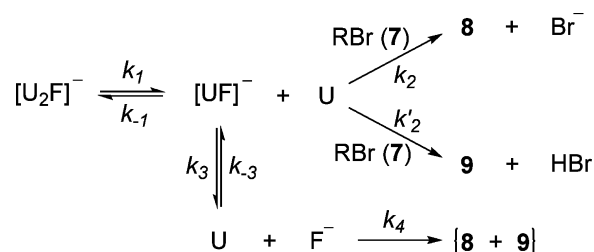


**Figure 9.** Collective analysis of N(H)⋯F<sup>−</sup> distances for the X-ray structures described in this paper, by donor category. Only the major components of the disordered structures 2g and 2k are included.

was 4.2:1 in favor of substitution. Three of the complexes involved were *bis*-chelating diols, each providing four H-bonds to fluoride with an average O(H)⋯F<sup>−</sup> distance of RMS = 2.615 ± 0.021 Å. Since this is shorter than the corresponding average distance in 2:1 1,3-diaryleurea complexes, it was of considerable interest to obtain comparative reactivity data for the latter. Moreover, since several of these complexes are *p*-substituted, it affords additional information regarding ligand electronic effects on fluoride substitution chemistry with well-defined molecular complexes. The results obtained are recorded in Table 5. Also included in Table 5 are reactivity data from the amide complex 4 and squaramide complex 6a. The overriding feature from these experiments is that reactions of fluoride–urea complexes are slower than those of the previously published alcohol complexes. The proportion of alkene formed by competing E2 elimination is also much lower. At long reaction times, side reactions were observed that depleted the reactant 7 without leading to either 8 or 9. For this reason, reaction progress (as measured by <sup>1</sup>H NMR of aliquots taken from the reaction mixture) was subsequently modeled as product formation vs time through curve fitting using Berkeley Madonna software (see SI for details). Entries 1–10 (Table 5) show that there is a general trend of decreasing reactivity with increasing electron-withdrawing character in the aryl ring substituent. This is qualitative, since the halide substituents in 2h and 2j are comparable in reactivity to the parent 2e, and 4-CF<sub>3</sub> (2b) is more deactivating than 4-NO<sub>2</sub> (2c). Electron withdrawal is associated with higher levels of chemoselectivity: >8:1, greater than any selectivity observed elsewhere in the literature for this procedure.<sup>3c</sup> These results are consistent with the higher acidity of 2c and 2b and hence the stronger H-bonds likely to be formed from the parent ureas. The spread of S<sub>N</sub>2 reactivity is relatively small, about 8-fold across the full range of substituents.

Just as had been observed with alcohol–fluoride complexes,<sup>9</sup> the second-order rate constants increase significantly with dilution (Table 5, entries 5 and 6 vs entry 4). This strongly implies that dissociation of one urea is normally needed to produce a reactive 1:1 urea–fluoride species, but further dissociation is discouraged at this concentration as indicated by the high levels of chemoselectivity observed compared to free fluoride (Table 5, entry 13). Given the concurrent loss of chemoselectivity for parent urea 2e with decreasing concentration, competition with further dissociation to a reactive free fluoride ion is probable at low [U<sub>2</sub>F]<sup>−</sup> concentration. The overall mechanism presented in eq 1 suggests a two-stage



process for which the pre-equilibrium  $K_1$  and reaction steps  $k_2$  will contribute to both turnover rate and chemoselectivity, with the highest selectivity being observed with the least reactive complex 2b (4-CF<sub>3</sub>) (Table 5, entry 10).

**III. Spectroscopic Analysis of Urea–Fluoride Binding.** The kinetic analyses mentioned above suggest that two sequential steps of dissociation may occur to provide more

**Table 5.** Reactions of Urea-, Amide-, and Squaramide-Fluoride Complexes with **7** in CH<sub>3</sub>CN (Conditions: (X)<sub>2</sub>F<sup>-</sup> (0.4 mmol), **7** (0.2 mmol), CH<sub>3</sub>CN (0.8 mL), 70 °C)

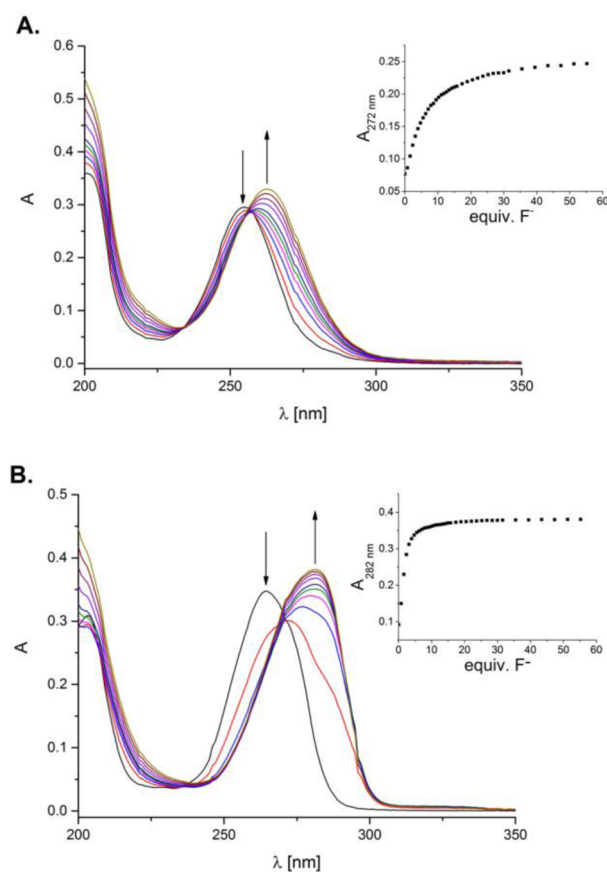
entry <sup>a</sup>	complex	$k_2(\text{S}_{\text{N}}2)^b$ [ $\times 10^{-5} \text{ M}^{-1} \text{ s}^{-1}$ ]	$k'_2(\text{E}2)^b$ [ $\times 10^{-5} \text{ M}^{-1} \text{ s}^{-1}$ ]	$k_2(\text{S}_{\text{N}}2)/k'_2(\text{E}2)^c$
1; 4-OMe	<b>2g</b>	12.7	2.45	5.2
2; 4-Me	<b>2f</b>	9.8	1.65	5.7
3; 3-Me	<b>2a</b>	5.95	1.07	5.6
4; H	<b>2e</b>	5.76	0.85	6.8
5; H <sup>d</sup>	<b>2e</b>	18.8	4.63	4.1
6; H <sup>e</sup>	<b>2e</b>	42.4	12.9	3.3
7; 4-F	<b>2j</b>	5.67	0.80	7.1
8; 4-Cl	<b>2h</b>	5.83	0.84	6.9
9; 4-NO <sub>2</sub>	<b>2c</b>	3.2	0.38	8.4
10; 4-CF <sub>3</sub> <sup>f</sup>	<b>2b</b>	1.65	0.19	8.7
11 <sup>g</sup>	<b>4</b>	178	112	1.6
12 <sup>g,h</sup>	<b>6a</b>	(2)	(0.7)	2.8
13 <sup>h</sup>	TBAF·3H <sub>2</sub> O	375	235	1.6

<sup>a</sup>Substituent of urea. <sup>b</sup>From <sup>1</sup>H NMR analysis by curve fitting. <sup>c</sup>For comparison, the ratio  $k_2(\text{S}_{\text{N}}2)/k'_2(\text{E}2)$  for TBAF·4(*t*-BuOH) was 2.1 (see ref 9). <sup>d</sup>0.0625 M. <sup>e</sup>0.025 M. <sup>f</sup>In a separate reaction under identical conditions, yields of **8** and **9** after 48 h were determined to be 45% and 4%, respectively, using <sup>19</sup>F and <sup>1</sup>H NMR with 1-fluoro-3-nitrobenzene as internal reference. <sup>g</sup>See Table 4. <sup>h</sup>Slow reaction accompanied by decomposition of diamide **5a**.

active fluoride species that react as either a nucleophile or base. We examined urea complexation of fluoride ion in solution to gain further insight. It is known that the process results in changes in the UV/visible region, and our first objective was thus to study the effects of changes in the electronic character of the 1,3-diarylureas. At first, UV-vis titrations of 8.0 μM solutions of selected ureas in MeCN, with a TBAF solution whose exact concentration had previously been established using a known method,<sup>30</sup> were performed without changing the urea concentration over the course of the addition (Figure 10). A bathochromic shift of the band with a maximum between 250–264 nm was observed, and the buildup of the absorption at the new maximum between 259–282 nm was plotted against the concentration of added fluoride. Association constants,  $K_{a,1:1}$ , that assumed the formation of a 1:1 urea-fluoride complex were obtained (eq 2, Table 6) via nonlinear least-squares regression using DynaFit4 software, forming the basis of the Hammett plot of Figure 11, with a  $\rho$ -value (vs  $2\sigma_p$ ) for the process of  $0.43 \pm 0.03$ .<sup>31</sup> Free energies of complexation  $\Delta G_{1:1}$  ranged from 23.3–28.1 kJ/mol.



In the case of electron-rich 1,3-diarylureas, assuming the formation of a 1:1 urea-fluoride complex as the only product gave good results, with the presence of two isosbestic points also indicating the clean transition between two structures (see Figure 10A). Band deconvolution analysis also showed the presence of two species over the course of the titration (see Figure S22). For electron-deficient 1,3-diarylureas, on the other hand, the behavior was more complex and lacked a clean isosbestic point (Figure 10B). Here, band deconvolution suggested the formation of a third species, which becomes predominant at higher F<sup>-</sup> concentrations (see Figures S38–S39). Taking the early data points in the titration (up to ca. 10 equiv), a reasonable fit to the 1:1 model was obtained; at higher concentrations of F<sup>-</sup> the results deviated from this. The UV-vis spectra of the 4-nitrophenylurea **1c** in the presence of various anions had been studied previously; for fluoride this was

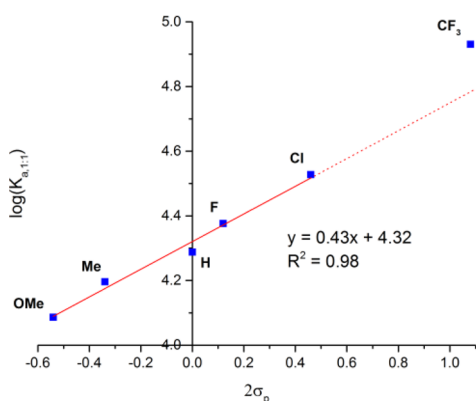


**Figure 10.** (A) Series of UV-vis spectra: 8.0 μM **1e** (4-H) (MeCN) vs 1.58 mM TBAF·3H<sub>2</sub>O. Inset: Titration profile, 272 nm. (B) Same for **1b** (4-CF<sub>3</sub>). Inset: Titration profile, 282 nm.

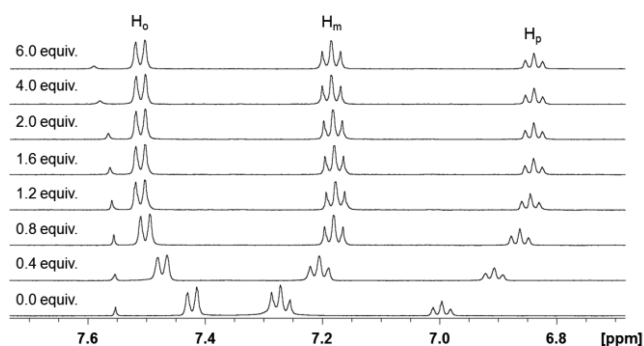
dominated by a band at 475 nm associated with the deprotonated species.<sup>32</sup> This is a likely possibility in the present case for the more N–H acidic examples, particularly 4-CF<sub>3</sub> substituted **1b**.<sup>33</sup>

Table 6. Association Constants  $K_{a,1:1}$  and Free Energies  $\Delta G_{1:1}$  for the Formation of  $[UF]^-$  Complexes

	4-H (1e)	4-Me (1f)	4-OMe (1g)	4-F (1j)	4-Cl (1h)	4-CF <sub>3</sub> (1b)
$\log(K_{a,1:1}) [M^{-1}]$	4.29(1)	4.20(2)	4.09(2)	4.38(2)	4.53(2)	4.93(1)
$\Delta G_{1:1} [kJ mol^{-1}]$	24.5(1)	24.0(1)	23.3(1)	25.0(1)	25.8(1)	28.1(1)

Figure 11. LFER based on the results of UV–vis titrations of 1,3-diarylureas with TBAF·3H<sub>2</sub>O in MeCN.

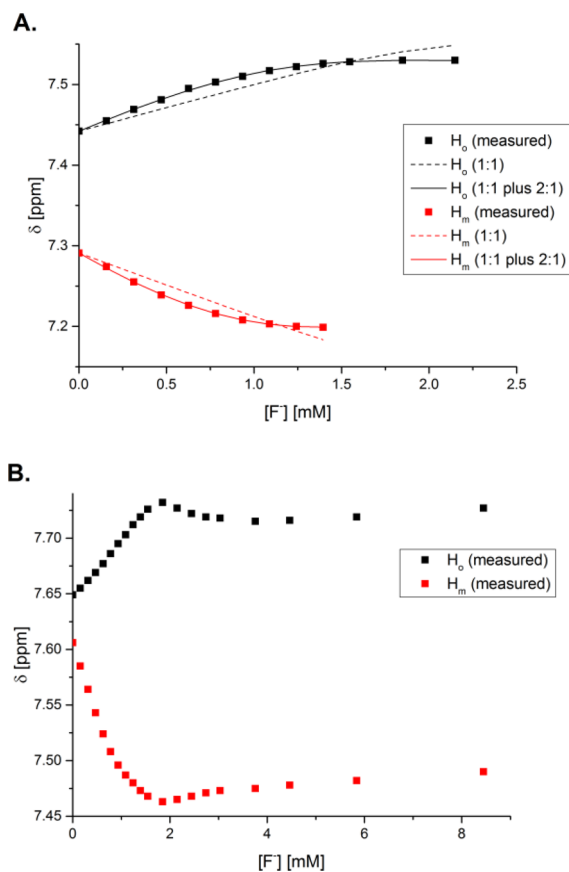
Having established the formation of 1:1 urea–fluoride complexes for a range of *para*-substituted 1,3-diarylureas through UV–vis spectroscopy in the  $\mu M$  range, we performed similar <sup>1</sup>H NMR titrations with a starting urea concentration of 1–2 mM. The possibility of 2:1 complexation comparable to the crystalline state was considered at this higher concentration. Increasing TBAF addition to the urea solution in CH<sub>3</sub>CN/CD<sub>3</sub>CN led to a pronounced downfield shift of the broadened N–H proton signal, with an asymptote between 1.0 and 1.5 equiv of added fluoride depending on the structure of the urea. For the more electron-deficient ureas, this signal was invisible at >1.0 equiv of added fluoride. Systematic changes also occurred in all aromatic protons, reflecting the same fluoride-binding process, with deshielding of *ortho*-protons, and shielding of *meta*- and *para*-protons by ca. 0.1 ppm over the range of added TBAF (Figure 12). This observation can be rationalized with an

Figure 12. A series of <sup>1</sup>H NMR spectra: 2.0 mM 1e (H) (CH<sub>3</sub>CN/CD<sub>3</sub>CN, 8:2) vs 78.9 mM TBAF·3H<sub>2</sub>O.

increased electron density in the phenyl rings via through-bond propagation upon fluoride binding exerting a shielding influence on all aromatic protons. *Ortho*-protons, however, are also affected by a dominant deshielding through-space effect.

Analysis of the aromatic signal shifts was carried out as for the UV–vis data, but did not fit the simple 1:1 model that applied there. When the possibility of 2:1 complexation was

included in the model a good fit was obtained across the range of substituted ureas (Figure 13A). The concentration of this

Figure 13. (A) Fitting of 1:1 and (1:1 + 2:1) binding model to C–H chemical shifts taken from a series of <sup>1</sup>H NMR spectra for sequential TBAF·3H<sub>2</sub>O (78.9 mM in 8:2 CH<sub>3</sub>CN/CD<sub>3</sub>CN) addition to 1e (4-H) (2 mM in 8:2 CH<sub>3</sub>CN/CD<sub>3</sub>CN). (B) C–H chemical shifts taken from a series of <sup>1</sup>H NMR spectra for sequential TBAF·3H<sub>2</sub>O (78.9 mM in 8:2 CH<sub>3</sub>CN/CD<sub>3</sub>CN) addition to 1b (4-CF<sub>3</sub>) (2 mM in 8:2 CH<sub>3</sub>CN/CD<sub>3</sub>CN).

second 2:1 complex, presumably structurally related to the X-ray-defined species, reached a maximum at 0.5 equiv of fluoride and decayed subsequently. This made it possible to determine association constants  $K_{a,2:1}$  and free energies  $\Delta G_{2:1}$  for the formation of these 2:1 complexes from their 1:1 precursors for more electron-rich ureas (eq 3, Table 7).<sup>31</sup>

Table 7. Association Constants  $K_{a,2:1}$  and Free Energies  $\Delta G_{2:1}$  for the Formation of  $[U_2F]^-$  Complexes

	4-H (1e)	4-Me (1f)	4-OMe (1g)
$\log(K_{a,2:1}) [M^{-1}]$	2.4(1)	2.7(1)	2.40(6)
$\Delta G_{2:1} [kJ mol^{-1}]$	13.6(8)	15.3(6)	13.7(3)



Deviations in the model were observed for electron-withdrawing substituents, however, particularly  $\text{CF}_3$  (Figure 13B). In these cases the plateau declined steadily with increasing fluoride concentration, with the more complex behavior mirroring that observed in the UV-vis titrations.

Since the reagent used was commercially available  $\text{TBAF}\cdot 3\text{H}_2\text{O}$ , this afforded the possibility of competing water complexation for the fluoride ion. This was checked in two ways: (1) by deliberately adding water as part of the sequence, and (2) by mixing the anhydrous complex **2e** and corresponding 1,3-diphenylurea **1e** in appropriate ratios to independently reproduce points of the titration. These experiments demonstrated conclusively that urea **1e** binds the fluoride ion sufficiently strongly to out-compete water, even when water is present in considerable excess (Figure 14). Association constants are therefore referenced to  $(\text{F}^- \cdot 3\text{H}_2\text{O})$ , not anhydrous fluoride.

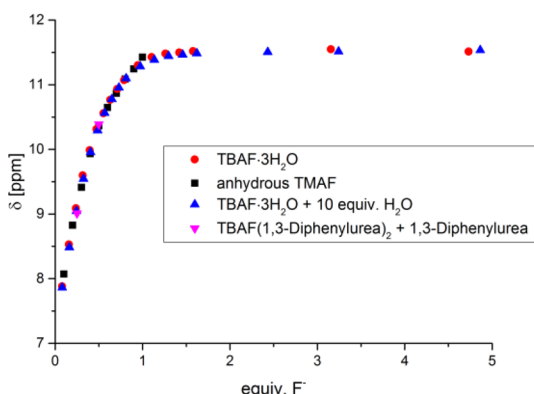


**Figure 14.** Proton chemical shift of N–H as a function of added fluoride ( $\text{TBAF}\cdot 3\text{H}_2\text{O}$ : 78.9 mM in 8:2  $\text{CH}_3\text{CN}/\text{CD}_3\text{CN}$ ;  $\text{TMAF}$ : 100 mM in anhydrous  $\text{DMSO}$ ) for parent urea **1e** (2 mM in 8:2  $\text{CH}_3\text{CN}/\text{CD}_3\text{CN}$ ) with and without addends, as in caption.

Additional evidence for the formation of  $[\text{UF}]^-$  and  $[\text{U}_2\text{F}]^-$  complexes in solution resulted from  $^1\text{H}$  diffusion-ordered NMR spectroscopy (DOSY) experiments performed in  $\text{CD}_3\text{CN}$ .<sup>34</sup> The diffusion coefficient,  $D$ , of free unsubstituted urea **1e** was found to be  $(2.09 \pm 0.02) \times 10^{-9} \text{ m}^2 \text{ s}^{-1}$ . Upon addition of  $\text{TBAF}\cdot 3\text{H}_2\text{O}$  this value, now corresponding to the averaged urea species in solution, decreased until it reached a minimum of  $(1.64 \pm 0.01) \cdot 10^{-9} \text{ m}^2 \text{ s}^{-1}$  after 0.5 equiv of fluoride had been added. This shows an increase in the hydrodynamic radius of the average urea molecule, caused by the formation of hydrogen-bonded adducts. On further addition,  $D$  then began to increase until 1.5 equiv of fluoride had been added, before reaching a plateau at  $(1.75 \pm 0.02) \cdot 10^{-9} \text{ m}^2 \text{ s}^{-1}$ , demonstrating a decrease in the average hydrodynamic radius on going from 0.5 to 1.5 equiv of fluoride. Comparing these results with the species distribution calculated from the previously determined association constants,  $K_{a,1:1}$  and  $K_{a,2:1}$ , for **1e** using the HYPERQUAD software package showed good agreement with initial formation of a mixture of  $[\text{UF}]^-$  and  $[\text{U}_2\text{F}]^-$  followed by consumption of this species in favor of the former (Figure 15).<sup>35</sup>

The successful characterization of 1,3-bis(4-fluorophenyl)-urea complex **2j** by neutron diffraction analysis enables precise determination of the average  $\text{NH}\cdots\text{F}^-$  distance in the solid state ( $1.732 \pm 0.068 \text{ \AA}$ ). For comparison, 1D  $^{19}\text{F}$ – $^1\text{H}$  heteronuclear NOE (HOESY) analysis was performed on the urea–fluoride

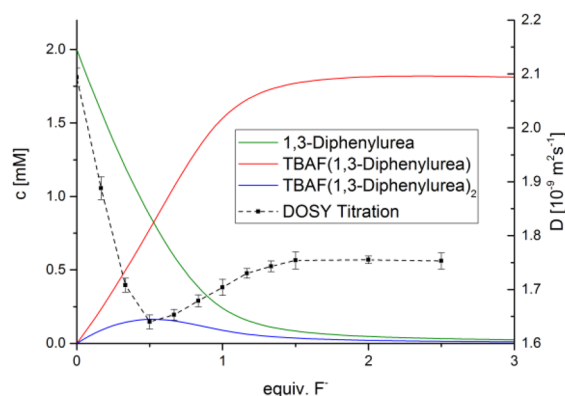


**Figure 15.** Simulated species distribution and diffusion coefficient,  $D$ , over course of titration of 1,3-diphenylurea **1e** (2 mM in  $\text{CD}_3\text{CN}$ ) with  $\text{TBAF}\cdot 3\text{H}_2\text{O}$  (81.1 mM in  $\text{CD}_3\text{CN}$ ). Error bars show standard deviation determined from three independent experiments.

complex **2j** to estimate the distance between the urea N–H and  $\text{F}^-$  in the solution phase.<sup>36</sup> Estimates of  $^1\text{H}$ – $^{19}\text{F}$  internuclear separations were made through comparison of  $^{19}\text{F}$ – $^1\text{H}$  NOE intensities with those observed between proton–fluorine pairs of known internuclear distance using the isolated spin-pair (initial rate) approximation<sup>37</sup> and assuming isotropic molecular tumbling occurs in solution. The average aryl *meta*-H–*para*-F distance of  $2.599 \pm 0.012 \text{ \AA}$ , as determined from the neutron structural data, provided a standard. Heteronuclear NOE build-up curves for both  $^1\text{H}$ – $^{19}\text{F}$  pairs were recorded to identify the region in which the initial-rate approximation was valid and the slopes of the linear build-up were determined.<sup>38</sup>

The  $\text{NH}\cdots\text{F}^-$  distance in **2j** was found to be  $1.86 \pm 0.01 \text{ \AA}$  in the relatively nonpolar solvent  $\text{DCM}-d_2$ . This distance compares with  $1.732 \pm 0.068 \text{ \AA}$  derived from neutron diffraction. In more polar solvents the same procedure led to greater attenuation, however, with values of  $2.03 \pm 0.01 \text{ \AA}$  ( $\text{DMSO}-d_6$ ),  $2.23 \pm 0.01 \text{ \AA}$  ( $\text{THF}-d_8$ ), and  $2.42 \pm 0.01 \text{ \AA}$  ( $\text{MeCN}-d_3$ ) respectively. These data indicate that more complex behavior is involved for this fast-exchanging species in more polar media that are also potential competing H-bond donors.

## CONCLUSION

This work presents a large set of data on the synthesis, structure, and reactivity of homoleptic complexes of ureas, amides, and squaramides with fluoride in the solid state and in solution. The results are instructive at various levels.

In the solid state, a surprisingly rich diversity of structural arrangements is observed. For urea ligands, complexes other than the documented  $[\text{U}_2\text{F}]^-$  system have been prepared and characterized featuring both tetra- and hexacoordinate fluoride complexes. In the tetracoordinate series, structural variations include supramolecular structure of the type  $[\text{U}_4\text{F}_2]^{2-}$  and systems cocrystallizing with water  $[\text{U}_2(\text{H}_2\text{O})_2\text{F}_2]^{2-}$ . The nature of the counteraction can impose structural changes as exemplified with the synthesis and characterization of hexacoordinate fluoride complexes surrounded by three urea ligands  $[\text{U}_3\text{F}]^-$  that are formed when  $\text{TBA}^+$  is replaced with either  $\text{TMA}^+$  ( $\text{Me}_4\text{N}^+$ ) or  $\text{TEA}^+$  ( $\text{Et}_4\text{N}^+$ ). An additional complex where fluoride has six short hydrogen contacts was found in the homoleptic complex  $[\text{A}_2\text{F}]^-$  ( $\text{A} = \text{amide}$ ) derived from  $N,2,2$ -triphenylacetamide. This structure is of interest as the fluoride makes weak hydrogen-bonding contacts with both

the phenyl C–H and benzyl C–H bonds, in addition to strong hydrogen bonding with the amide N–H functionality. Further structural variations are obtained from squaramide complexes, more particularly the unusual 1D ribbon structure of type  $\{[(\text{H}_2\text{O})_2\text{FSq}]^-\}_n$ . To the best of our knowledge, this structural diversity is unprecedented and offers new opportunities in the multidisciplinary fields of supramolecular chemistry and catalysis.<sup>39</sup> For complexes derived from bromo- and iodo-containing ureas, an additional point of interest resides in the presence of both hydrogen- and halogen-bonding contacts.

For the first time, urea–fluoride complexes are considered here as reagents for C–F bond formation. Nucleophilic substitution of a model alkyl bromide is possible with these new complexes, and the reaction is found to be significantly slower in comparison with known alcohol–fluoride complexes. A major advantage of the novel urea complexes described here is their ability to favor  $\text{S}_{\text{N}}2$  vs E2 at a level surpassing all hydrogen-bonded complexes documented in the literature. As a spur for future progress, we note that high selectivity in  $\text{S}_{\text{N}}2$  chemistry is achieved at the expense of reactivity. The enzymatic reactivity of fluorinase lowers the energy  $\Delta^\ddagger E$  of nucleophilic substitution by an estimated factor of 39  $\text{kJ mol}^{-1}$ , according to QM/MM calculations.<sup>5d</sup> The most striking “reactivity and selectivity” trend is best manifested with the strongly hydrogen-bonded fluoride complex derived from 1,3-bis(4-(trifluoromethyl)phenyl)urea. Increased second-order rate constants together with reduced selectivity at higher dilution supports the hypothesis that the reactive species is a partially dissociated  $[\text{UF}]^-$  complex that dissociates further at lower concentration to give free fluoride ion.

Experimental results based on UV–vis titration indicate that the strength of the urea–fluoride complex is tunable by modifying substituents on the urea receptor. Hammett LFE analysis indicates a positive  $\rho$  value; hence stronger binding is seen with electron-deficient aryl groups. Further analysis by  $^1\text{H}$  NMR spectroscopy provides direct evidence for the presence of both  $[\text{UF}]^-$  and  $[\text{U}_2\text{F}]^-$  complexes in solution as a function of fluoride ion concentration. A striking result is the ability of urea to outcompete water for hydrogen bonding to fluoride.

The first single-crystal neutron diffraction studies of urea–fluoride complexes provide accurate information on  $\text{NH}\cdots\text{F}^-$  distances in the solid state. This allows for direct comparison with experimental values in different solvents that were derived from HOESY experiments.

Hydrogen bonding to fluoride is an interaction that has seen increasing applications in anion sensing, organocatalysis, molecular/ion recognition, and more recently as a tool to modulate reactivity in the context of C–F bond formation. New methods for diversifying, understanding, and controlling the strength and selectivity of these interactions are therefore vital for further developments in these fields to materialize. From our perspective, the results from this study provide important insights to explore how these interactions can lead to adaptable fluoride reagents, with the ultimate aim being control of reactivity and product selectivity for transformations other than the  $\text{S}_{\text{N}}2$ :E2 scenario selected in this study.

## EXPERIMENTAL SECTION

For the preparation of TBAF–urea complexes, a flame-dried flask was charged with TBAF·3H<sub>2</sub>O (2.0 mmol), the according urea (4.0 mmol), and hexane (60 mL) before refluxing the mixture for 2 h. During this time the formation of water droplets on the inside walls of the condenser is observed. After cooling to rt, solvents were

removed *in vacuo* to give solid products, which were placed on a filter, washed with hexane, and dried under high vacuum to obtain clean TBAF–urea complexes. Single crystals suitable for X-ray analysis were obtained by recrystallization from THF, EtOAc, or DCM by reducing solubility in a saturated solution through slow mixing with hexane using a layering or vapor diffusion technique. See the [Supporting Information](#) for details regarding individual compounds.

Low temperature (150 K) single-crystal X-ray diffraction data<sup>40</sup> were collected using either a Nonius Kappa CCD diffractometer or an Oxford Diffraction (Agilent) SuperNova A diffractometer and reduced using the appropriate instrument manufacturer supplied software.<sup>41</sup> Structures were solved using either SIR92<sup>42</sup> or SuperFlip<sup>43</sup> and refined using full-matrix least-squares refinement with CRYSTALS.<sup>44</sup> On refinement of **2b** it became apparent that the CF<sub>3</sub> groups were disordered. A multicomponent model proved to be inadequate, so the major component was modeled with conventional anisotropic displacement parameters and the residual electron density was fitted as described by Schröder et al.<sup>45</sup> Structure **2k** was found to exhibit diffuse disordered solvent which was modeled using PLATON/SQUEEZE.<sup>46,47</sup> C⋯F<sup>−</sup> distances, N(H)⋯F<sup>−</sup> distances, F<sup>−</sup>⋯F<sup>−</sup> distances, dihedral angles, DHA angles, and O⋯F<sup>−</sup>⋯O angles were calculated using PLATON,<sup>46,48</sup> and N–H and NH⋯F<sup>−</sup> distances were calculated with CRYSTALS using the full variance-covariance matrix though they were displayed herein using Mercury.<sup>49</sup> Neutron diffraction data were collected at several orientations at 150 K in a top-loading closed-cycle refrigerator on the SXD time-of-flight Laue diffractometer at the ISIS spallation neutron source.<sup>50</sup> Data were reduced using SXD 2001,<sup>51</sup> and the atomic positions obtained from the X-ray solutions were refined against the neutron data using SHELXL.<sup>52</sup>

For further details see the full crystallographic data (in CIF format) which are available Associated Content and have been deposited with the Cambridge Crystallographic Data Centre (reference codes CCDC 1493410–1493434); these data can also be obtained free of charge via [www.ccdc.cam.ac.uk/data\\_request/cif](http://www.ccdc.cam.ac.uk/data_request/cif).

## ASSOCIATED CONTENT

### Supporting Information

The Supporting Information is available free of charge on the ACS Publications website at DOI: 10.1021/jacs.6b07501.

Experimental details and data (PDF)

Crystallographic data (CIF)

## AUTHOR INFORMATION

### Corresponding Author

\*[veronique.gouverneur@chem.ox.ac.uk](mailto:veronique.gouverneur@chem.ox.ac.uk)

### Present Addresses

<sup>§</sup>Department of Chemistry, The Scripps Research Institute, 10550 North Torrey Pines Road, La Jolla, California 92037, United States.

<sup>||</sup>School of Chemistry, University of Bristol, Cantock's Close, BS8 1TS Bristol, United Kingdom.

### Notes

The authors declare no competing financial interest.

## ACKNOWLEDGMENTS

The authors thank the European Union (FP7-PEOPLE-2012-ITN-RADIOMI-316882 to L.P.), the Skaggs-Oxford Scholarship Program and NSF GRFP (predoctoral fellowships to K.M.E.) for generous funding. V.G. thanks the Royal Society for a Wolfson Research Merit Award (2013–2018). We are grateful to Prof. Tim D. W. Claridge for help with the DOSY and HOESY studies, the ISIS spallation neutron source for the allocation of beam time and Dr. Matthias J. Gutmann for help with neutron data collection and processing.

## REFERENCES

- (1) (a) Preshlock, S.; Tredwell, M.; Gouverneur, V. *Chem. Rev.* **2016**, *116*, 719. (b) Campbell, M. G.; Ritter, T. *Chem. Rev.* **2015**, *115*, 612. (c) Yang, X.; Wu, T.; Phipps, R. J.; Toste, F. D. *Chem. Rev.* **2015**, *115*, 826. (d) Hollingworth, C.; Gouverneur, V. *Chem. Commun.* **2012**, *48*, 2929.
- (2) Harsanyi, A.; Sandford, G. *Green Chem.* **2015**, *17*, 2081.
- (3) (a) Emsley, J. *Chem. Soc. Rev.* **1980**, *9*, 91. (b) Adams, D. J.; Clark, J. H. *Chem. Soc. Rev.* **1999**, *28*, 225. (c) Lee, J.-W.; Oliveira, M. T.; Jang, H. B.; Lee, S.; Chi, D. Y.; Kim, D. W.; Song, C. E. *Chem. Soc. Rev.* **2016**, *45*, 4638.
- (4) (a) O'Hagan, D.; Schaffrath, C.; Cobb, S. L.; Hamilton, J. T. G.; Murphy, C. D. *Nature* **2002**, *416*, 279. For examples of formal C–F bond formation by mutant enzymes, see: (b) Nashiru, O.; Zechel, D. L.; Stoll, D.; Mohammadzadeh, T.; Warren, R. A. J.; Withers, S. G. *Angew. Chem., Int. Ed.* **2001**, *40*, 417. (c) Zechel, D. L.; Reid, S. P.; Nashiru, O.; Mayer, C.; Stoll, D.; Jakeman, D. L.; Warren, R. A. J.; Withers, S. G. *J. Am. Chem. Soc.* **2001**, *123*, 4350.
- (5) (a) O'Hagan, D.; Deng, H. *Chem. Rev.* **2015**, *115*, 634. (b) Dong, C.; Huang, F.; Deng, H.; Schaffrath, C.; Spencer, J. B.; O'Hagan, D.; Naismith, J. H. *Nature* **2004**, *427*, 561. (c) Zhu, X.; Robinson, D. A.; McEwan, A. R.; O'Hagan, D.; Naismith, J. H. *J. Am. Chem. Soc.* **2007**, *129*, 14597. (d) Senn, H. M.; O'Hagan, D.; Thiel, W. *J. Am. Chem. Soc.* **2005**, *127*, 13643.
- (6) Vincent, M. A.; Hillier, I. H. *Chem. Commun.* **2005**, 5902.
- (7) (a) Yonezawa, T.; Sakamoto, Y.; Nogawa, K. Preparation of Tetrabutylammonium Fluoride–Alcohol Adducts as Fluorination Agents. *Jpn. Kokai Tokkyo Koho*, 1994, JP 06316551 A. (b) Kim, D. W.; Jeong, H.-J.; Lim, S. T.; Sohn, M.-H.; Katzenellenbogen, J. A.; Chi, D. Y. *J. Org. Chem.* **2008**, *73*, 957. (c) Kim, D. W.; Ahn, D.-S.; Oh, Y.-H.; Lee, S.; Kil, H. S.; Oh, S. J.; Lee, S. J.; Kim, J. S.; Ryu, J. S.; Moon, D. H.; Chi, D. Y. *J. Am. Chem. Soc.* **2006**, *128*, 16394. (d) Kim, D. W.; Jeong, H.-J.; Lim, S. T.; Sohn, M.-H. *Tetrahedron Lett.* **2010**, *51*, 432. (e) Kim, D. W.; Jeong, H.-J.; Lim, S. T.; Sohn, M.-H. *Angew. Chem., Int. Ed.* **2008**, *47*, 8404. (f) Yan, H.; Jang, H. B.; Lee, J.-W.; Kim, H. K.; Lee, S. W.; Yang, J. W.; Song, C. E. *Angew. Chem., Int. Ed.* **2010**, *49*, 8915. (g) Hollingworth, C.; Hazari, A.; Hopkinson, M. N.; Tredwell, M.; Benedetto, E.; Huiban, M.; Gee, A. D.; Brown, J. M.; Gouverneur, V. *Angew. Chem., Int. Ed.* **2011**, *50*, 2613. (h) Benedetto, E.; Tredwell, M.; Hollingworth, C.; Khotavivattana, T.; Brown, J. M.; Gouverneur, V. *Chem. Sci.* **2013**, *4*, 89.
- (8) For other approaches, see: (a) Kim, D. W.; Song, C. E.; Chi, D. Y. *J. Am. Chem. Soc.* **2002**, *124*, 10278. (b) Pliego, J. R., Jr.; Pilo-Veloso, D. *J. Phys. Chem. B* **2007**, *111*, 1752. (c) Lu, S.; Lepore, S. D.; Li, S. Y.; Mondal, D.; Cohn, P. C.; Bhunia, A. K.; Pike, V. W. *J. Org. Chem.* **2009**, *74*, 5290.
- (9) Engle, K. E.; Pfeifer, L.; Pidgeon, G. W.; Giuffredi, G. T.; Thompson, A. L.; Paton, R. S.; Brown, J. M.; Gouverneur, V. *Chem. Sci.* **2015**, *6*, 5293.
- (10) (a) Bregović, V. B.; Basarić, N.; Mlinarić-Majerski, K. *Coord. Chem. Rev.* **2015**, *295*, 80. (b) Amendola, V.; Boiocchi, M.; Colasson, B.; Fabbri, L. *Inorg. Chem.* **2006**, *45*, 6138. (c) Brooks, S. J.; Gale, P. A.; Light, M. E. *Chem. Commun.* **2006**, 4344. (d) Gómez, D. E.; Fabbri, L.; Licchelli, M.; Monzani, E. *Org. Biomol. Chem.* **2005**, *3*, 1495.
- (11) (a) Xu, S.-Y.; Sun, X.; Ge, H.; Arrowsmith, R. L.; Fossey, J. S.; Pascu, S. I.; Jiang, Y.-B.; James, T. D. *Org. Biomol. Chem.* **2015**, *13*, 4143. (b) Raju, M. V. R.; Lin, H.-C. *Org. Lett.* **2013**, *15*, 1274. (c) Elmes, R. B. P.; Turner, P.; Jolliffe, K. A. *Org. Lett.* **2013**, *15*, 5638. (d) Amendola, V.; Bergamaschi, G.; Boiocchi, M.; Fabbri, L.; Mosca, L. *J. Am. Chem. Soc.* **2013**, *135*, 6345. (e) Duke, R. M.; Gunnlaugsson, T. *Tetrahedron Lett.* **2011**, *52*, 1503.
- (12) Steed, J. W. *Chem. Soc. Rev.* **2010**, *39*, 3686.
- (13) Etter, M. C.; Urbanczyk-Lipkowska, Z.; Zia-Ebrahimi, M.; Panunto, T. W. *J. Am. Chem. Soc.* **1990**, *112*, 8415.
- (14) (a) Zhang, Z.; Schreiner, P. R. *Chem. Soc. Rev.* **2009**, *38*, 1187. (b) Auvil, T. J.; Schafer, A. G.; Mattson, A. E. *Eur. J. Org. Chem.* **2014**, *2014*, 2633. (c) Beckendorf, S.; Asmus, S.; Mancheño, O. G. *ChemCatChem* **2012**, *4*, 926.
- (15) Custelcean, R.; Jiang, D.-E.; Hay, B. P.; Luo, W. S.; Gu, B. H. *Cryst. Growth Des.* **2008**, *8*, 1909.
- (16) (a) Ravikumar, I.; Lakshminarayanan, P. S.; Arunachalam, M.; Suresh, E.; Ghosh, P. *Dalton Trans.* **2009**, 4160. (b) Kormos, A.; Móczár, I.; Pál, D.; Baranyai, P.; Holczbauer, T.; Palló, A.; Tóth, K.; Huszthy, P. *Tetrahedron* **2013**, *69*, 8142. (c) Li, M.; Wu, B.; Jia, C.; Huang, X.; Zhao, Q.; Shao, S.; Yang, X.-J. *Chem. - Eur. J.* **2011**, *17*, 2272. (d) Paul, M.; Adarsh, N. N.; Dastidar, P. *Cryst. Growth Des.* **2012**, *12*, 4135.
- (17) Kirby, I. L.; Brightwell, M.; Pitak, M. B.; Wilson, C.; Coles, S. J.; Gale, P. A. *Phys. Chem. Chem. Phys.* **2014**, *16*, 10943.
- (18) For example, the NNCO interplanar angle is 4.26(15)° in **2c**, but 40.30(3)° in the known Me<sub>4</sub>N<sup>+</sup> analogue: Kirby, I. L.; Pitak, M. B.; Wenzel, M.; Wilson, C.; Sparkes, H. A.; Coles, S. J.; Gale, P. A. *CrystEngComm* **2013**, *15*, 9003.
- (19) Desiraju, G. R.; Sarma, J. A. R. P. *Proc. - Indian Acad. Sci., Chem. Sci.* **1986**, *96*, 599.
- (20) Herbststein, F. H. *Crystalline Molecular Complexes and Compounds*, Vol. I; Oxford University Press: Oxford, 2005; p 606.
- (21) Allen, F. *Acta Crystallogr., Sect. B: Struct. Sci.* **2002**, *58*, 380.
- (22) (a) Metrangolo, P.; Meyer, F.; Pilati, T.; Resnati, G.; Terraneo, G. *Angew. Chem., Int. Ed.* **2008**, *47*, 6114. (b) Politzer, P.; Murray, J. S.; Clark, T. *Phys. Chem. Chem. Phys.* **2013**, *15*, 11178.
- (23) This structure is believed to be modulated (see SI); the average structure is included in this study for completeness, but the full modulated description is being submitted for publication separately.
- (24) As an isolated unit: Emsley, J.; Arif, M.; Bates, P. A.; Hursthouse, M. B. *J. Chem. Soc., Chem. Commun.* **1989**, 738.
- (25) Further examples, often as part of a larger cluster: (a) Dalapati, S.; Akhtarul Alam, M.; Saha, R.; Jana, S.; Guchhait, N. *CrystEngComm* **2012**, *14*, 1527. (b) Trzybiński, D.; Sikorski, A. *CrystEngComm* **2013**, *15*, 6808. (c) Vreugdenhil, W.; Birker, P. J. M. W. L.; ten Hoedt, R. W. M.; Verschoor, G. C.; Reedijk, J. *J. Chem. Soc., Dalton Trans.* **1984**, 429. (d) Li, Q.; Mak, T. C. W. *Acta Crystallogr., Sect. B: Struct. Sci.* **1998**, *54*, 180.
- (26) Jones, C. R.; Baruah, P. K.; Thompson, A. L.; Scheiner, S.; Smith, M. D. *J. Am. Chem. Soc.* **2012**, *134*, 12064.
- (27) (a) Garau, C.; Frontera, A.; Ballester, P.; Quiñonero, D.; Costa, A.; Deyà, P. M. *Eur. J. Org. Chem.* **2005**, *2005*, 179. (b) Amendola, V.; Bergamaschi, G.; Boiocchi, M.; Fabbri, L.; Milani, M. *Chem. - Eur. J.* **2010**, *16*, 4368. (c) Alemán, J.; Parra, A.; Jiang, H.; Jørgensen, K. A. *Chem. - Eur. J.* **2011**, *17*, 6890. (d) Gaeta, C.; Talotta, C.; Della Sala, P.; Margarucci, L.; Casapullo, A.; Neri, P. *J. Org. Chem.* **2014**, *79*, 3704.
- (28) Elmes, R. B. P.; Turner, P.; Jolliffe, K. A. *Org. Lett.* **2013**, *15*, 5638.
- (29) Busschaert, N.; Kirby, I. L.; Young, S.; Coles, S. J.; Horton, P. N.; Light, M. E.; Gale, P. A. *Angew. Chem., Int. Ed.* **2012**, *51*, 4426.
- (30) Sokkalingam, P.; Lee, C.-H. *J. Org. Chem.* **2011**, *76*, 3820.
- (31)  $K_{a,1,1}$  and  $K_{a,2,1}$  values were obtained by fitting of a binding model by nonlinear least-squares regression using the DynaFit 4 software package: Kuzmič, P. *Anal. Biochem.* **1996**, *237*, 260.
- (32) Boiocchi, M.; Del Boca, L.; Gomez, D. E.; Fabbri, L.; Licchelli, M.; Monzani, E. *J. Am. Chem. Soc.* **2004**, *126*, 16507.
- (33) It is to be noted here that addition of TBAOH to an 8 μM solution of **1b** in MeCN also led to the formation of an absorption peak coinciding with the supposed deprotonated species.
- (34) (a) Jerschow, A.; Müller, N. *J. Magn. Reson.* **1997**, *125*, 372. (b) Claridge, T. D. W. *High-resolution NMR Techniques in Organic Chemistry*; Elsevier: Amsterdam, 2016; p 381 ff. For a recent application to anion binding, see: (c) Toure, M.; Charles, L.; Chendo, C.; Viel, S.; Chuzel, O.; Parrain, J.-L. *Chem. - Eur. J.* **2016**, *22*, 8937.
- (35) Gans, P.; Sabatini, A.; Vacca, A. *Talanta* **1996**, *43*, 1739.
- (36) (a) Combettes, L. E.; Clausen-Thue, P.; King, M. A.; Odell, B.; Thompson, A. L.; Gouverneur, V.; Claridge, T. D. W. *Chem. - Eur. J.* **2012**, *18*, 13133. Recent examples of NMR HOESY analyses: (b) Ciancaleoni, G.; Belpassi, L.; Tarantelli, F.; Zuccaccia, D.; Macchioni, A. *Dalton Trans.* **2013**, *42*, 4122. (c) Rocchigiani, L.;

Ciancaleoni, G.; Zuccaccia, C.; Macchioni, A. *J. Am. Chem. Soc.* **2014**, *136*, 112.

(37) (a) Neuhaus, D.; Williamson, M. P. *The Nuclear Overhauser Effect in Structural and Conformational Analysis*, 2nd ed.; Wiley: New York, 2000. (b) Butts, C. P.; Jones, C. R.; Towers, E. C.; Flynn, J. L.; Appleby, L.; Barron, N. J. *Org. Biomol. Chem.* **2011**, *9*, 177.

(38) Distances were then calculated as  $r_{\text{NH}\cdots\text{F}} = r_{\text{mH}\cdots\text{pF}} [s_{\text{NH}\cdots\text{F}} / s_{\text{mH}\cdots\text{pF}}]^{-1/6}$  in which  $r_{\text{NH}\cdots\text{F}}$  is the distance to be determined,  $r_{\text{mH}\cdots\text{pF}}$  the reference distance, and  $s_{\text{NH}\cdots\text{F}}$  and  $s_{\text{mH}\cdots\text{pF}}$  the corresponding slopes of the linear build-up curves.

(39) Upon addition of 20 mol% of **1b** to a reaction of **7** with 2.0 equiv of CsF the yield of **8** improved from 7% to 46%, as determined by  $^{19}\text{F}$  and  $^1\text{H}$  NMR using 1-fluoro-3-nitrobenzene as an internal reference (see SI).

(40) Cosier, J.; Glazer, A. M. *J. Appl. Crystallogr.* **1986**, *19*, 105.

(41) Otwinowski, Z.; Minor, W. Processing of X-ray Diffraction Data Collected in Oscillation Mode. In *Methods in Enzymology*; Carter, C. W., Jr., Sweet, R. M., Eds.; Academic Press: New York, 1997; Vol. 276, pp 307–326.

(42) Altomare, A.; Cascarano, G.; Giacovazzo, C.; Guagliardi, A.; Burla, M. C.; Polidori, G.; Camalli, M. *J. Appl. Crystallogr.* **1994**, *27*, 435.

(43) Palatinus, L.; Chapuis, G. *J. Appl. Crystallogr.* **2007**, *40*, 786.

(44) (a) Betteridge, P. W.; Carruthers, J. R.; Cooper, R. I.; Prout, K.; Watkin, D. J. *J. Appl. Crystallogr.* **2003**, *36*, 1487. (b) Cooper, R. I.; Thompson, A. L.; Watkin, D. J. *J. Appl. Crystallogr.* **2010**, *43*, 1100. (c) Parois, P.; Cooper, R. I.; Thompson, A. L. *Chem. Cent. J.* **2015**, *9*, 30. (d) Thompson, A. L.; Watkin, D. J. *J. Appl. Crystallogr.* **2011**, *44*, 1017.

(45) Schröder, L.; Watkin, D. J.; Cousson, A.; Cooper, R. I.; Paulus, W. *J. Appl. Crystallogr.* **2004**, *37*, 545.

(46) Spek, A. L. *J. Appl. Crystallogr.* **2003**, *36*, 7.

(47) van der Sluis, P.; Spek, A. L. *Acta Crystallogr., Sect. A: Found. Crystallogr.* **1990**, *46*, 194.

(48) Spek, A. L. *PLATON, A Multipurpose Crystallographic Tool*; Utrecht University: Utrecht, The Netherlands, 1998.

(49) Macrae, C. F.; Bruno, I. J.; Chisholm, J. A.; Edgington, P. R.; McCabe, P.; Pidcock, E.; Rodriguez-Monge, L.; Taylor, R.; van de Streek, J.; Wood, P. A. *J. Appl. Crystallogr.* **2008**, *41*, 466.

(50) Keen, D. A.; Gutmann, M. J.; Wilson, C. C. *J. Appl. Crystallogr.* **2006**, *39*, 714.

(51) Gutmann, M. J. *Acta Crystallogr., Sect. A: Found. Crystallogr.* **2005**, *61*, C164.

(52) Sheldrick, G. M. *Acta Crystallogr., Sect. A: Found. Crystallogr.* **2008**, *64*, 112.